31st Congress of the International Council of the Aeronautical Sciences

Belo Horizonte, Brazil; September 09-14, 2018

DESIGN AND PERFORMANCE ASSESSMENT OF AN INVERTED RECTANGULAR DORSAL INTAKE FOR MILITARY AVIATION

Pedro David Bravo-Mosquera*, Alvaro Martins Abdalla*, Hernán Darío Cerón-Muñoz*, Fernando Martini Catalano*

* **Department of Aeronautical Engineering, São Carlos Engineering School, University of São Paulo, Brazil**

Keywords: *Dorsal intake, S-duct, Boundary layer diverter, RANS, Air-to-Ground fighter*

Abstract

This paper aims to design and analyze an inverted dorsal intake for military aircraft applications with adequate efficiency in a wide range of operating conditions. The configuration of the intake was modeled after analytic and numerical analysis, resulting in a supersonic diffuser with rectangular cross section and external compression, followed by a three dimensional transitioning S-duct diffuser with circular cross section at exit plane. In addition, a swept wedge-type boundary layer diverter and a bleed system with porous wall were designed in order to integrate the intake over an air-to-ground fighter aircraft. Reynolds-averaged Navier-Stokes simulations are conducted to understand effects of propulsion-airframe integration on the flow field around the intake and the aircraft. The main results found in this work shown that appropriate performance and compatibility characteristics were maintained during subsonic and transonic flight simulations. However, for supersonic velocities, the flow expansion on the fuselage and wings produced an increase in the local Mach number into the intake entrance, which reduced its performance levels. These features infer that dorsal intakes are a promising alternative for aircraft that require only reasonable supersonic maneuverability capabilities and high subsonic and transonic capabilities.

1 General Introduction

Aircraft conception with dorsal intake configurations arose in the 1960s due to investigations performed about new design features that could be used on the military vehicles of that time. This led to propose an aircraft that mixes the interceptor and the fighter-bomber capabilities [1]. Nowadays, this unconventional intake position continues to be used on aircraft designed for several applications, such as Unmanned Aerial Vehicles (UAVs), heavy bombers, silent supersonic technology demonstrators, supersonic business jet and, in our case, an air-to-ground fighter aircraft. Following the previous idea, the most relevant advantages of this position include: a low radar signature by integrating the engine into the aircraft using an S-duct diffuser, which prevents direct radar line-of-sight to the engine face, unobstructed lower-fuselage for more weapons integration capabilities, which also eliminates engine-intake compatibility problems during weapons load and delivery, reduction of the incidence of foreign objects damage (FOD) inside the engines, which reduce maintenance cost and reduction of the aircraft structural weight due to the decrease of the duct length [2-5].

On the other hand, advanced and current studies have suggested that inverting the intakes upside-down regarding the flow direction aids to

obtain more compression effects by the fuselage and the flow diverter, which allows to control and stabilize the normal shock wave just inside the cowl lip. In this way, the fraction of air spilled around the intake is a minimum and the intake is said to be "matched" to the engine [6-8]. In addition, this configuration presents a lower external drag coefficient due to the changed pressure distribution between the inverted intake cowl and the boundary layer diverter, when compared to non-inverted intake configurations [9]. Finally, inverted intakes can enhance the performance at high angles of attack due to the mass flow rate remains constant and then, the total pressure recovery decreases in a limited range [9-11]. This is the reason why some experimental aircraft with dorsal-inverted intakes are being designed, such as the TsAGI SSBJ concept [12, 13] and the SSBJ/SSCJ [14, 15].

Nevertheless, this non-conventional configuration presents several constraints that must be overcome in order to be installed on any aircraft successfully. For example, there is the necessity of a suppression method to reduce the interaction between intake shock waves and fuselage boundary layer. Therefore, the efficient design of an adequate boundary layer diverter is undoubtedly, the most important parameter to be considered for designing and integrating a dorsal-inverted intake on an aircraft.

In sum, the objective of this paper is to conceptually explore the inverted rectangular dorsal intake characteristics that could expand the capabilities of an air-to-ground fighter aircraft, called F/AB-31 "Bravo". Before proceeding, it is necessary to determine the condition to design the intake, therefore, the "Escape-Dash" phase according to a typical mission profile of an air-to-ground fighter was selected (On-design condition). In this phase, aircraft usually accelerate to a high-speed dash of Mach = 2 at which, a common jet engine loses 8% of the free stream total pressure through the intake, suffering a thrust reduction of 13% and consequently an increase of 5% in fuel consumption [16]. For these reasons, in an attempt to improve the relation between intake pressure recovery and aircraft wave drag, the intake was modified to create a non-conventional one.

The intake design is comprised of two separate methods: an analytic-parametric tool for sizing the intake geometry and high-fidelity CFD-based analysis for accurate performance evaluation and improvement of intake-airframe integration of dorsal configurations. In the present study, several flight conditions were assessed, including supersonic, transonic and subsonic velocities, as well as a wide range of angles of attack.

2 Brief description of the military aircraft under study

An air-to-ground fighter aircraft is a tactical military aircraft that has the primary mission of carrying out airstrikes with greater precision than bombers. This class of aircraft is designed to encounter strong low-level air defenses while pressing the attack, i.e. most of the aircraft are designed for close air support and naval air-to-surface missions, overlapping the tactical bomber capabilities [17].

The aircraft presented in this work has been designed following the framework of aeronautical engineering as defined by Whitford [16], Roskam [18] and Raymer [19], i.e. the conceptual, preliminary and detailed phases. Each phase has its own characteristic, involving aerodynamics, propulsion, and structural design, which restrict the entire aircraft design process. In this case, a special tool was developed in order to perform a step-by-step analysis of the conceptual design phase of the F/AB-31 aircraft, where the most important parameter is defining the design requirements of it.

In case of ground support (or attack) aircraft, whose primary task is the destruction of enemy logistics and/or support for ground troops under fire, some design requirements and objectives include: short take-off and landing distances for quick military operation, high Thrust-to-Weight (T/W) ratio, as it helps in low altitude maneuverability in order to quick ingress and egress from the combat area; high weapons load capacity, as it enables engagement of a large number of tar-

gets; a reduced radar cross section (RCS), as it decreases the distance at which the enemy can detect the aircraft using radar; ruggedness, as the aircraft should be able to take some amount of punishment and return to base station; high range and endurance on target, as the ground troops may require support for an extended period of time, with corresponding weapons load; and high supersonic speed for quick escape dash and evasion [20, 21]. Table 1 summarizes some design requirements established for the F/AB-31 Bravo aircraft.

Table 1 Design requirements of F/AB-31 Bravo.

Requirement	Performance
Take-off distance	$\leq$ 500 m
Cruise speed	Mach 1.2-1.4
Escape dash	Mach 2
Rate of climb	254 m/s
Supersonic turn	Mach 1.5 at 5 g-load
Subsonic turn	Mach 0.8 at 5 g-load
Acceleration	Mach 0.8 to 1.5, $\Delta_t \leq 50$ s
Landing	$\leq$ 500 m
MTOW	14000 Kg

Most of the design requirements presented above are related to the flight phases that the aircraft is to be designed for. Therefore, the application of the constraint analysis allowed to calculate the main performance characteristics of the aircraft in relation to each phase of flight. Those characteristics are: the Wing Loading (W/S) and the Thrust to Weight Ratio (T/W), which means that, the required thrust, the wing geometry and the weights distribution are the parameters that have the greatest influence on engine performance, fuel consumption and the maximum cross-section area of the aircraft. After computations, the design point of the F/AB-31 aircraft minimized the engine power and also the wing loading, which reduce the fuel consumption and enhance its aerodynamic characteristics. The design point of the F/AB-31 aircraft was set at T/W = 0.92 and W/S = 415 Kg/m^2, which represent a non-installed thrust (T = 126.3 kN) and wing area (S = 34.1 m^2) according to its Maximum Take-off Weight (MTOW). More specific details are found in Bravo-Mosquera [22]. The F/AB-31 aircraft is shown in Fig. 1.

Fig. 1 F/AB-31 "Bravo" aircraft.

3 Aerodynamic design of the intake

The intake in a jet propulsion system must satisfy an essential requirement; decelerate and compress the incoming airflow to subsonic speeds for entry into the engine [7]. This airflow should be free of distortions, stable and be able to transform most of the kinetic energy into energy due to pressure [8]. Therefore, a correct estimation of the number of ramps needed to reduce the relative velocity of the aircraft was developed, followed by an S-shaped subsonic diffuser to make viscous loss small as possible by setting optimal area distribution. In addition, the process of intake-airframe integration must be developed by designing an efficient boundary layer diverter and a bleed system to improve the aerodynamic performance of the intake by removing the boundary layer developed on the fuselage and ramps.

To design the intake, it should be considered that the thrust value obtained by the constraint analysis represents only the ideal performance of the engine, in the sense that it corresponds to an installation without external drag. Therefore, assembling the engine within the airframe inevitably induces forces on the external surfaces (intake and nozzle) that increase the total drag, commonly called "self-drag" forces [23]. These additional forces, as were appointed by Goldsmith and Seddon [7] must be counterbalanced

by added uninstalled thrust. Exclusively the external loss coefficient of the intake and nozzle were considered for each flight condition of the aircraft mission requirements. As the nozzle is not the focus of this study, the loss coefficient of it ($\phi_{No} = 0.03$) were added considering a propulsion system with similar characteristics [23].

The analytic estimation of the external loss coefficient of the intake (ϕ_{In}) was calculated regarding the Eq. (1) and assuming that the intake is operating at critical condition (Ideal), see Fig. (2).

$$\phi_{In} = \frac{\left(\frac{A_1}{A_0} - 1\right)\left[M_0 - \left(\frac{2}{\gamma+1} + \frac{\gamma-1}{\gamma+1}M_0^2\right)^{1/2}\right]}{[F g_c/(\dot{m}_0 a_0)]} \quad (1)$$

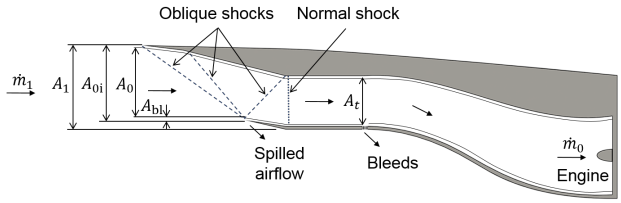

Fig. 2 Intake system operating at its critical condition.

where A_1 represents the capture area of the entire admission system, A_{0i} is the area of the supersonic diffuser, A_0 is the cross-sectional area in the engine entrance, A_{bl} is the boundary layer bleed area, A_t is the throat area, $F/\dot{m}_0$ is the specific thrust when the engine is not installed on the aircraft, a_0 is the sound velocity and g_c is the Newton's gravitational constant.

In the current design phase, two assumptions should be done. The intake area A_1 must be sized to accept slightly more airflow than the engine requires in order to prevent internal boundary layer separation. In addition, the bypass and bleed flows must return to the free-stream with velocities that are sonic and aligned with the free-stream velocity. This suggests that A_1 must simply exceed the largest required A_0 by the minimum amount needed for boundary layer bleed and margin of safety. The amount of boundary layer bleed depends on the intake type and design shape [7, 8], and, for this case, it will be about 4% to account for external compression intake. Therefore, $A_1 = 1.04A_0$ [23].

Once A_1 has been selected, the Eq. (1) can be directly evaluated at any given flight condition (i.e., a_0 and M_0) and engine power setting (i.e., A_0 and $F/\dot{m}_0$). The minimum engine size required is that for which allows that the uninstalled thrust (T_u) be approximate to the required installed thrust (T_r) for the most demanding flight conditions, i.e. $[(T/W)_r/(T/W)_u \approx 1]$. In this context, the required installed thrust was calculated considering the installation penalties of the intake and nozzle using the following expression:

$$T_r = T_u\,(1 - \phi_{In} - \phi_{No}) \quad (2)$$

Table 2 summarizes the process to select the engine, considering the self-drag forces, the design requirements and the design point of the F/AB-31 aircraft.

Table 2 Engine required thrust loading $(T/W)_r$ for $(T/W)_u = 0.92$.

Requirement	M_0	$T_u[kN]$	$\phi_{In}+\phi_{No}$	$T_r[kN]$	$\left(\frac{T}{W}\right)_r$	$\frac{(T/W)_r}{(T/W)_u}$
Take-off	0.1	124.7	0.0142	123	0.89	0.97
Cruise speed	1.4	106.5	0.043	101.8	0.74	0.8
Escape dash	2.0	125.3	0.047	119.3	0.86	0.94
Supersonic turn	1.5	131.3	0.039	126.1	0.91	0.99
Subsonic turn	0.8	91.9	0.017	90.3	0.65	0.71
Acceleration	1.2	126	0.019	123.5	0.89	0.97

Checking engines that accomplish these requirements, and after tradeoffs studies among safety, performance, and cost, the Pratt & Whitney F100-229 engine was selected to be used in the aircraft.

3.1 Supersonic diffuser

The preliminary design of the supersonic diffuser aims to optimize the performance of the P&W F100-229 engine. This is achieved by providing a correct quantity and quality of mass flow into the engine. An adequate estimation of the number of shock waves needed to reduce the relative velocity of the air was developed (station point 1 to 4 of Fig. 3). This is a non-isentropic process due to frictional effects and shock waves, which manifests itself as a loss of total pressure [24]. However, the total pressure recovery (η_R)

was maximized by selecting an adequate number of compression ramps. For this purpose, a MATLAB program was developed following the charts of compressible flow presented in Anderson [25] and Barnhart [26]. The code is characterized by using two computational package in order to find the ramp angles and areas ratio that minimize the total pressure loss through the intake. The first package calculates the shock angle (θ), using Mach and ramp angles (δ) as inputs. The second package determines the static pressure, total pressure and Mach downstream of the shock waves by considering upstream conditions, which can easily be evaluated assuming adiabatic and isentropic flow. The aforementioned approach was an iterative process in which two compression ramps and the cowl angle were varied from $\delta = 0^o$ to 20^o, until find the optimal configuration. The outline of the supersonic region of the intake is shown in the Fig. 3. It is observed that its geometry is formed by the solution of the compressible flow normal and oblique shock relations at On-design condition.

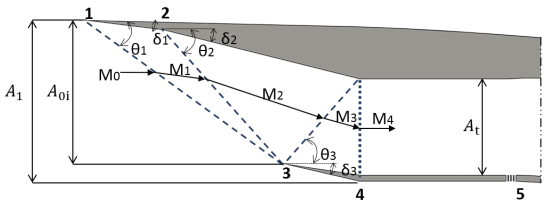

Fig. 3 Geometry of the supersonic diffuser at On-design condition.

After iterative computations, the external air compression system consists of two ramps with deflection angles of 7^o. The third ramp represents the cowl lip and was designed with straight leading edge and deflection angle of 8^o for matching the shocks at flowing over the swept bleeding wedge and also minimizing the cowl lip drag. The ramp angles provided the maximum theoretical total pressure recovery for the widest possible range of free stream Mach numbers, according to the military specification MIL-E-5008B [23].

After the shock system appears the throat (station point 4 to 5 of Fig. 3), which represents the transition zone that ensures the reattachment of the boundary layer after the terminal normal shock. Its area was calculated considering the generalized external compression geometry, from A_1 to A_t. Therefore, the inlet mass flow ratio was calculated as:

$$\frac{A_{0i}}{A_1} = \frac{A_{0i}}{A_t}\frac{A_t}{A_1} \tag{3}$$

where A_t/A_1 is determined by the geometry of the intake. The shock system determines the area ratio A_{0i}/A_t using conservation of mass, as follows:

$$\dot{m}_i = \dot{m}_t \tag{4}$$

thus

$$\frac{A_{0i}}{A_t} = \frac{\rho_t V_t}{\rho_0 V_0} \tag{5}$$

In this way, the ratio of density times velocity in Eq. 5 can be calculated in terms of the total pressure ratio and the Mach numbers using the mass flow parameter (MFP) and the isentropic area ratio (A/A^*) defined for a calorically perfect gas. Those terms are tabulated in many gas dynamics textbooks, such as [8, 23, 25, 26].

3.2 Subsonic diffuser

Once determined the geometry and the efficiency of the supersonic diffuser, analytic methodologies were implemented to the preliminary design of the subsonic diffuser (Fig. 4).

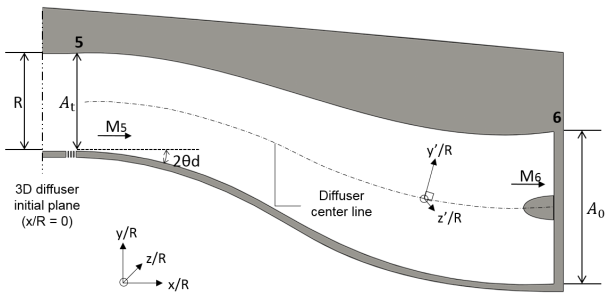

Fig. 4 Geometry of the subsonic diffuser at On-design condition.

Throughout the subsonic diffuser (station point 5 to 6 of Fig. 4), the flow field was solved

using a quasi-one-dimensional approach where the subsonic flow was diffused and decelerated to a higher static pressure and lower Mach number. As the intake is not aligned to the engine, a S-duct shape provided a smooth transition from the conditions at the throat to those required at the engine face, with minimal total pressure losses. At this point, two design specifications must be considered. For example, the engine face area was calculated from the circular fan face diameter minus the circular area of the spinner hub, i.e. (hub/tip) ratio [27]. Besides, the length of the subsonic diffuser must be directly specified as an input to match a specified expansion angle ($2\theta d$). In this case, the expansion angle is equal to 12^o to reduce expansion loss, enhance total pressure recovery and reduce the aircraft empty weight due to its short length.

The assessment of the total pressure recovery of the subsonic diffuser (PR_{sub}) was developed assuming that the total temperature is constant [28]. Then, its value was determined by the amount of viscosity losses through the S-duct using the Borda-Carnot loss equation, which is an empirical description of the mechanical energy losses of a fluid due to flow expansion [29, 30].

The total pressure recovery (η_R) at the engine face was determined as the product of the total pressure ratios among the stations throughout the entire intake, as shown in Eq. 6:

$$\eta_R = \prod_{i=1}^{3} PR_i \times PR_n \times PR_{sub} \tag{6}$$

where PR_i is evaluated as the total pressure losses through the oblique shock waves and PR_n is the total pressure loss downstream the terminal shock wave.

On the other hand, the subsonic diffuser changes its cross-sectional area from a rectangle (throat) to a circle (engine face) over its axial length, commonly known as "super-elliptical" shape [27-31]. Therefore, the diffuser center line (see Fig. 4) was sized regarding a fifth order polynomial in terms of (x/R) using the Eq. 7.

$$lc\left(\frac{x}{R}\right) = lc_0 + lc\left(\frac{x}{R}\right)_1 + lc\left(\frac{x}{R}\right)_2^2 + lc\left(\frac{x}{R}\right)_3^3 + \cdots \\ \cdots lc\left(\frac{x}{R}\right)_4^4 + lc\left(\frac{x}{R}\right)_5^5 \tag{7}$$

The constants of the last polynomial $\left(lc_{(x/R)}\right)$ were found according the method proposed by Wendt [31]. The first and second spatial derivatives were equaled to zero at the initial and exit duct boundaries. The super-elliptical cross-sections were defined by the following equation:

$$\frac{y'}{R} = b\left[1 - \left(\frac{z'}{R}\right)^n\right]^{1/n} \tag{8}$$

where (y'/R) and (z'/R) represent the orthogonal coordinate system showed in Fig. 4. The constants (b) and (n) are also fifth order polynomials in terms of (x/R), which were found in the same way as Eq. 7. In case of $\left(b_{(x/R)}\right)$, constants are obtained assuming that the diffuser bottom surface centerline has not curvature. The super-elliptical exponent $\left(n_{(x/R)}\right)$ controls the nature of the diffuser corners, therefore, constants of this polynomial are determined from an iterative fitting procedure to the desired cross-sectional area schedule of the diffuser. Fig. 5 depicts the 3D transitioning diffuser cross-sectional profiles at five axial stations spanning the length of this diffuser section.

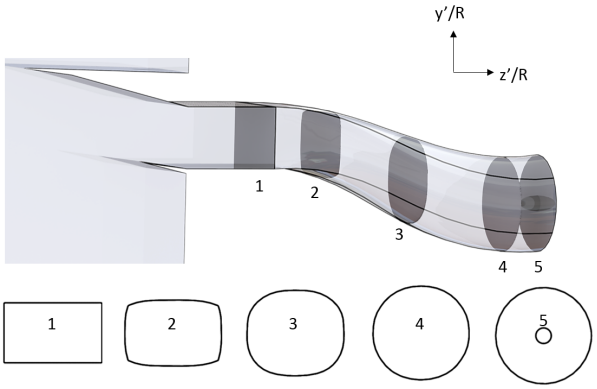

Fig. 5 Cross sections of the 3D transitioning diffuser section at six axial locations.

The final configuration of the preliminary design of the intake suggests that when the S-duct shape is combined with radar absorbing material,

the intake can effectively reduce the radar cross section of the aircraft [32, 33].

3.3 Boundary layer diverter and bleed system

Boundary layer control is a major design consideration in the design of supersonic intakes [6-8]. Since there is an adverse pressure gradient in the supersonic diffuser, the boundary layer is susceptible to separation when this pressure gradient is too severe, as can be the case when shock waves interact with the boundary layer [23]. To avoid this problem, active boundary layer diverters are used to remove most of the boundary layer just prior to the region where interaction with shocks occurs. In this case, both swept wedge-type boundary layer diverter and bleed system with porous wall are designed, as shown in Fig. 6.

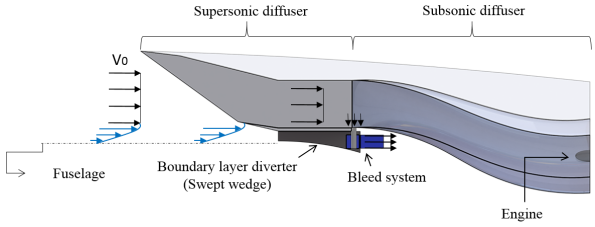

Fig. 6a. Side view.

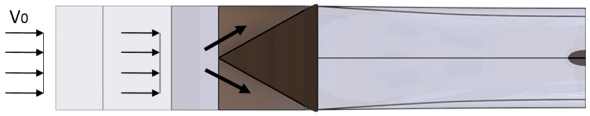

Fig. 6b. Bottom view.

Fig. 6 Intake design including boundary-layer diverter and bleed system

The swept wedge-type boundary layer diverter was designed to avoid the ingestion of the boundary layer developed at the top of the fuselage. Its cross-sectional area was restricted in relation to the afore-mentioned hypothesis ($A_1 = 1.04A_0$), allowing that ($\dot{m}_{bl}/\dot{m}_1 = A_{bl}/A_1$). As a result, this type of geometry changes the flow direction in lateral paths (see Fig. 6b), which causes a smaller pressure gradient in this region. Furthermore, the swept wedge reduces the drag produced by the integration of the propulsion system with the airframe, and stabilizes the position of the terminal normal shock within the intake [7, 19].

On the other hand, a porous bleed system was designed within the throat in order to decrease the intake flow rate between the inflow and outflow throat stations, improving the intake performance. Furthermore, bleed air prevents loss of total pressure when the intake is forced to work at supercritical operation. Bleed air is ejected from the bleed splines to outside, whose exit area is regulated by opening of about 5% of the capture area (see Fig. 6a). It should be noted that more than 5% may influence the sizing of the intake and enhance bleed drag [8, 24]. Further details concerning the intake design presented in section 3 may be obtained in Bravo-Mosquera [22].

4 Numerical Method

The numerical simulations of this study were carried out in order to assess and validate the performance of the designed intake before and after being mounted above the structure of the aircraft, i.e. on-design and off-design conditions were studied.

A finite-volume unstructured-grid Reynolds-Average-Navier-Stokes (RANS) solver is used in the current flow simulations. The compressible RANS equations are discretized by the cell-vertex finite volume method coupled with the Shear Stress Transport (SST) turbulence model. It combines the advantages of the original $k-\varepsilon$ and $k-\omega$ models by using the $k-\omega$ model near the wall, and the $k-\varepsilon$ model away from the wall [34].

At inlet boundary, the incoming flow properties were prescribed by the freestream flow at Mach number of 0.4, 0.9, 1.7 and 2.0. The outlet condition was imposed with no pressure gradient. No-slip and adiabatic wall conditions were imposed on the wall surfaces. Five porous bleed regions were located in the throat region to extract the 5% bleed specified in the design. Porous bleed boundary condition was modeled as outlet region with a uniform bleed flow rate model that

extracted a specified amount of flow through a bleed region defined by a patch of surface grid points.

For the engine face boundary condition, density and velocity properties from inside of the computational domain were extrapolated and a uniform static back pressure to match the target mass flow rate was imposed [27, 33, 35]. The mesh system was composed of structured and non-structured grid points. The structured grid was used to model viscous effects near the walls with boundary layers within normal distances of $Y^+ < 5$. However, the non-structured grid was used for the rest of the domain. Figure 7 shows the external and internal grid configuration on the integrated simulations. The analyses of this paper used grids containing about 4.2 million grid points. 1200 iterations were used in each simulation, using a maximum residual of $1e^{-}5$.

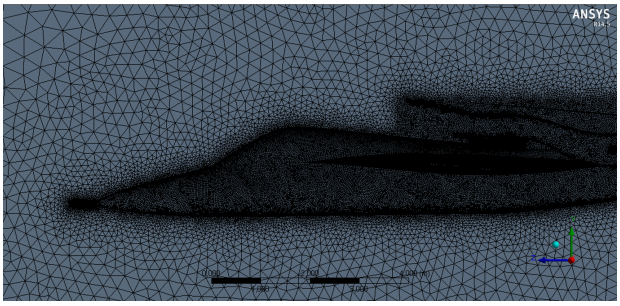

Fig. 7a. External grid.

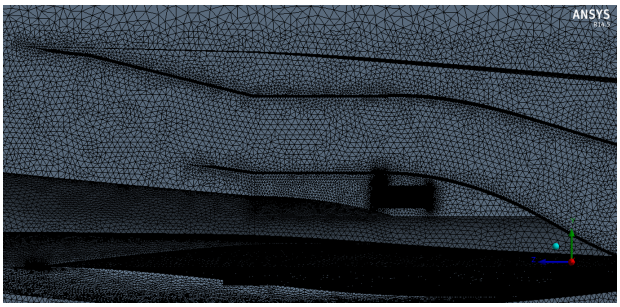

Fig. 7b. Internal grid.

Fig. 7 Computational mesh characteristics

5 Results and discussion

5.1 On-Design condition

The MATLAB code was used to determine the optimum ramp configuration for Mach numbers between Mach 1.0 to 2.0 at a pressure altitude of 10000 km and constant optimum subsonic diffuser.

Table 3 summarizes the main results for the optimization point of Mach 2.0. The ramp angles, shock wave angles, exit Mach numbers, pressure recovery (P_o/P_∞) and length values are listed.

Table 3 Intake properties at Mach = 2.0.

Supersonic diffuser					
Station	δ [deg]	θ [deg]	Mach	P_o/P_∞	Length [m]
1-2	7	36.2	1.74	0.994	0.381
2-3	7	41.87	1.5	0.995	0.55
3-4	8	52.11	1.21	0.993	0.379
Throat					
Station	Mach		P_o/P_∞		Length [m]
4-5	0.836		0.991		0.7
Subsonic diffuser					
Station	Mach		P_o/P_∞		Length [m]
5-6	0.67		0.983		2.25
Engine face	0.4		0.956		-

Likewise, the areas of the main sections of the intake are: $A_1 = 0.509m^2$, $A_{0i} = 0.464m^2$, $A_t = 0.335m^2$, $A_0 = 0.490m^2$.

On the other hand, all the performance results are compared to a On-Design condition CFD simulation in order to verify if the MATLAB code resuls are reliable (table 4).

Table 4 Intake performance summary.

	Analytical		**Numerical**	
Section	Mach	P_o/P_∞	Mach	P_o/P_∞
Freestream	2.0	1.0	2.0	1.0
Super-diffuser	1.21	0.982	1.22	0.979
Normal shock	0.83	0.973	0.85	0.970
Throat	0.83	0.991	0.85	0.991
Sub-diffuser	0.67	0.983	0.73	0.949
Engine face	0.4	0.956	0.45	0.941

The difference between analytical and numerical values is due to CFD provide increased level of detail and fidelity, as well as, complexity with the modeling of the turbulent boundary layers and their interactions with shock waves. However, the analytical model developed to design the intake presents reliable results when compared to numerical ones.

The above analysis demonstrated that the analytical design tool developed was well executed,

due to the shock wave formation occurred exactly where were designed. In addition, there were no significant pressure recovery losses. This is also possible to understand in Fig. 8. As can be seen, the normal shock is formed just at the beginning of the throat (critical operation). Therefore, this configuration provided the best mass flow quality to the engine.

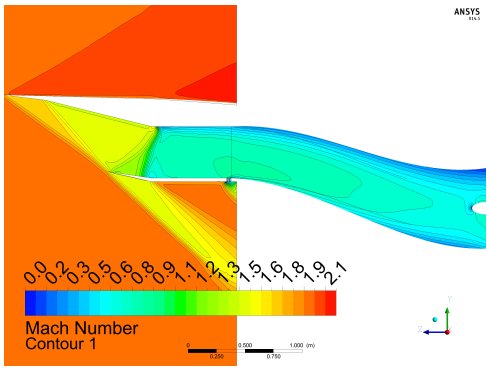

Fig. 8 Mach number contour at On-Design condition.

5.2 Intake-Airframe integration

The optimal intake was designed initially to deliver the best performance at the design point. Therefore, an additional study was conducted to analyze the intake performance during the integration on the airframe. The study focuses on the variation of the total pressure recovery and flow distortion of the intake for different flight conditions such as, flight Mach number and angle of attack (α). In this way, the total pressure recovery was calculated as Eq. 9, indicating the efficiency of the mass flow entering to the engine face.

$$\eta_R = \frac{P_e}{P_o} \tag{9}$$

where P_e represents the average total pressure at the engine face and P_o is the average total pressure of the freestream.

Flow distortion at fan faces can be quantified by calculating flow distortion indicators. The distortion index is described as Eq. 10.

$$DC_\theta = \frac{P_e - P_\theta}{q_e} \tag{10}$$

where P_θ is the mean total pressure on a 60^o sector that has the lowest mean recovery, and q_e is the mean dynamic pressure calculated by $q_e = P_o - P_s$, where P_s is the area-weighted average static pressure at the engine face. It should be noted that all data presented in this paper are for the maximum engine airflow condition.

The Mach number contour of the intake-airframe integration, along with a more detailed approximation of the intake geometry are shown in Fig. 9. In these figures, it is observed that a part of the expansion wave produced by the canopy and wings is ingested by the intake, as a consequence of the shock wave intensity generated on the upper surface of the fuselage. In this context, the total pressure recovery suffered a considerable reduction ($\eta_R = 0.84$) compared to the efficiency of the intake itself ($\eta_R = 0.941$).

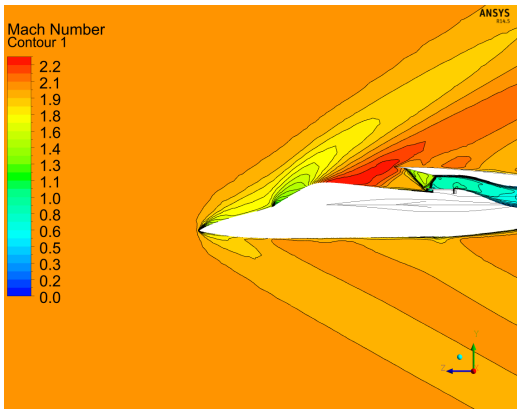

Fig. 9a. Mach number contour.

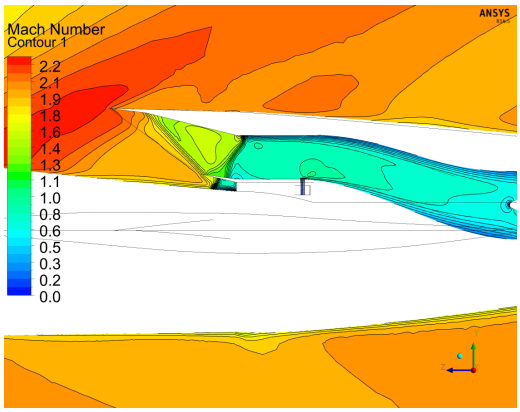

Fig. 9a. Approximation of the intake geometry.

Fig. 9 Mach number contour of the intake-airframe integration for Mach = 2.0.

Efficiency and compatibility intake variation of the intake-airframe integration in the four flight regimes studied is shown in Fig. 10.

It can be seen that for low angles of attack, the dorsal intake system exhibits high total pressure recovery levels and low distortion indexes, notwithstanding performance decreases with increasing Mach number. This is a result of the incidence of canopy-dorsal separation at low to moderate angles of attack, highlighting the importance of careful canopy-dorsal integration of dorsal intake installations.

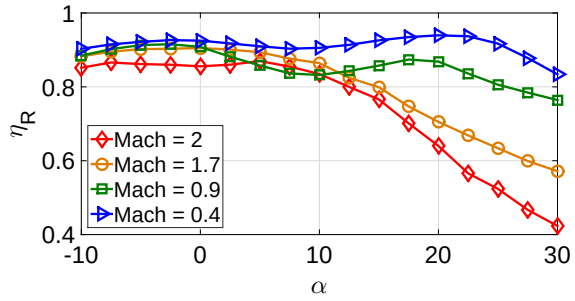

Fig. 10a. Total pressure recovery Vs α .

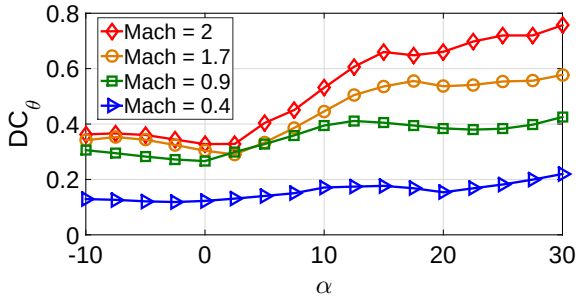

Fig. 10b. Distortion index Vs α.

Fig. 10 Total pressure recovery and Distortion index evaluated for the intake-airframe integration at Mach = 0.4, 0.9, 1.7, 2.0 for several α.

For supersonic velocities (Mach = 2 and 1.7), total pressure recovery is reduced as the angle of attack increase. As a result, the distortion index for both velocities is increased. This leads to a reduction in inlet recovery and increases the potential for engine-inlet compatibility problems.

Subsonic and transonic intake performance characteristics are also presented in Fig. 10. Note that from 0^o to 10^o, a general deterioration in total pressure recovery and distortion is obtained. This performance reduction resulted from the ingestion of low-energy flow emanated from the juncture of the wing leading edge extension and forebody. However, above $\alpha = 10^o$, a general improvement in the intake performance is evidenced. This effect is a result of the sweeping action of the vortex breakdown phenomena produced by the Leading Edge Extension (LEX) of the wing, which entrains the low-energy flow out the intake flow field, i.e. as the angle of attack increases, the leading edge of the wing generates a vortex which energizes the flow on the upper surface of the wing, delaying flow separation (see Fig. 11).

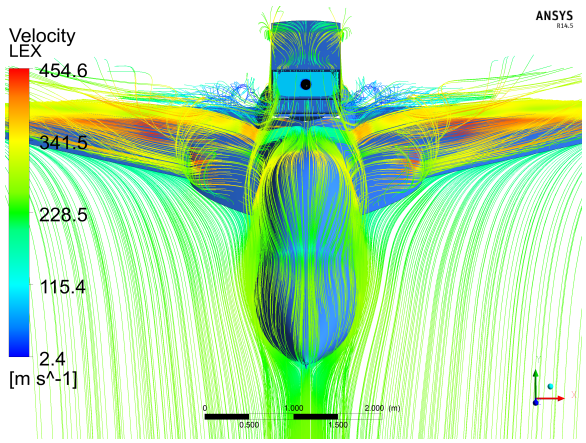

Fig. 11 Streamlines at Mach = 0.9 and $\alpha = 15^o$.

Fig. 12 and Fig. 13 show the comparisons of computational total pressure contours at the engine face for 0^o and 15^o, respectively. Clearly, ingested boundary layers are displayed, presenting greater thickness as Mach number and angle of attack increases. Therefore, all figures demonstrated the performance behavior obtained in Fig. 10.

6 Concluding remarks

In the present work, different methodologies were developed with the objective of designing a new concept of air-to-ground fighter aircraft, whose main characteristic is to have the air intake system in the upper surface of the fuselage. Throughout its development, the main perfor-

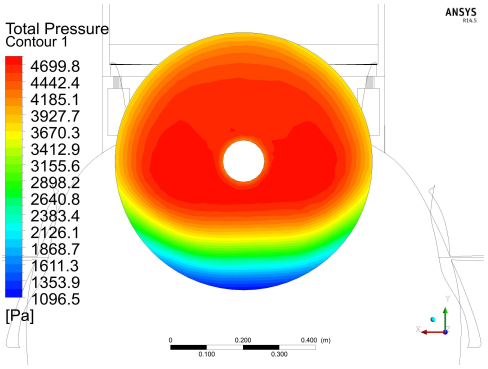

Fig. 12a. Mach number = 0.4.

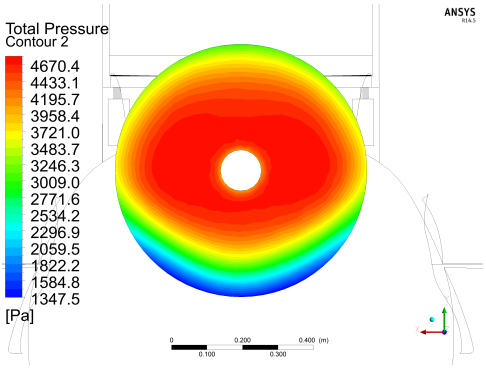

Fig. 13a. Mach number = 0.4.

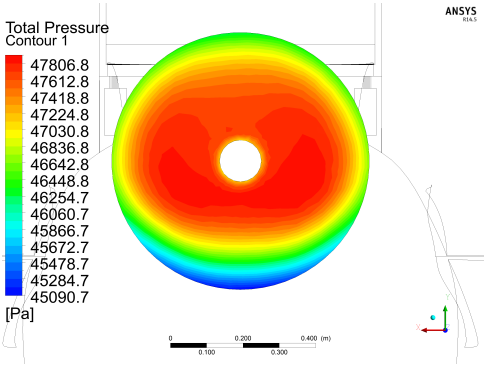

Fig. 12b. Mach number = 0.9.

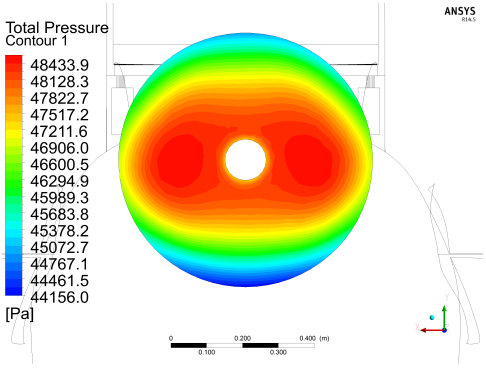

Fig. 13b. Mach number = 0.9.

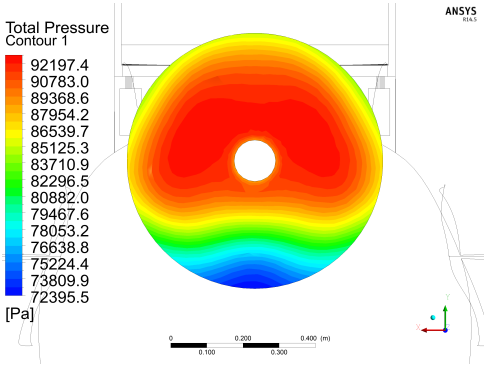

Fig. 12c. Mach number = 1.7.

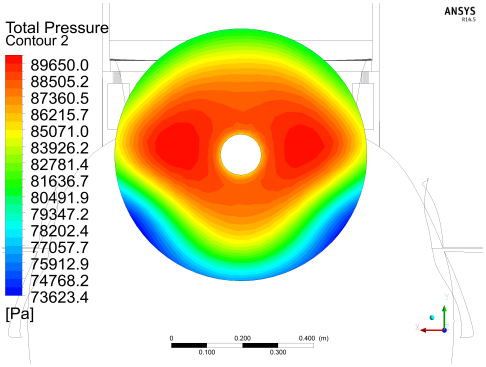

Fig. 13c. Mach number = 1.7.

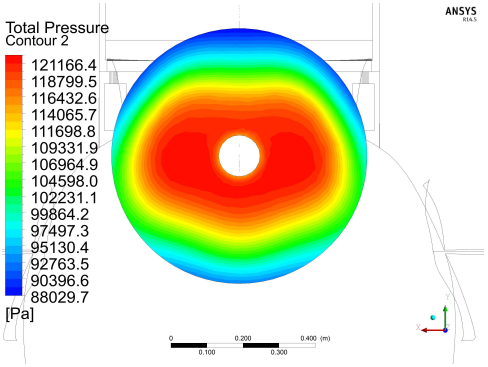

Fig. 12d. Mach number = 2.0.

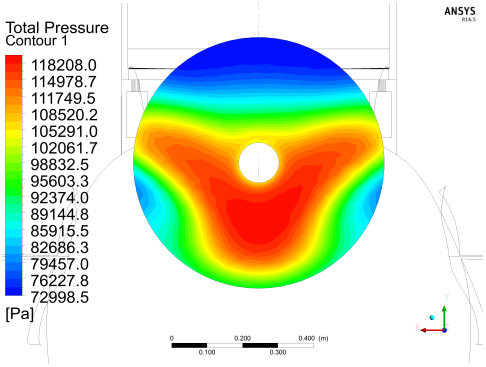

Fig. 13d. Mach number = 2.0.

Fig. 12 Total pressure contour at engine face, $\alpha = 0^o$ for different flight regimes.

Fig. 13 Total pressure contour at engine face, $\alpha = 15^o$ for different flight regimes.

mance characteristics that the aircraft must have in relation to its operating requirements were evaluated. Therefore, this evaluation was elaborated from the parametric design of the aircraft to the numerical design of the intake.

The preliminary design of the dorsal Intake presented appropriate aerodynamic characteristics at all stages of design and evaluation. Although the intake performance was evaluated under different design conditions, it showed appropriate levels of performance and compatibility with the selected engine. Therefore, the code developed for the design of the internal geometry of the intake was shown to be objective when compared to the existing techniques in the literature and CFD simulations.

The numerical analysis of the intake-airframe integration provided the most relevant results regarding the intake performance and the type of wing selected for the aircraft. Thus, for subsonic and transonic velocities, the dorsal intake configuration presented appropriate levels of performance in terms of efficiency and compatibility in the face of the selected engine, since the implementation of LEX devices improved the performance of the intake through the action of its vortices to delay and / or avoid the separation of the boundary layer at the top of the fuselage. The ingestion of low energy flow produced by the proper layout arrangement contributed negatively to the intake performance. For this reason, the choice of an appropriate wing configuration was of fundamental importance in improving intake performance conditions in all flight regimes.

At supersonic speeds for example, the dorsal intake configuration increased the local Mach number at the intake entrance for all evaluated angles of attack. Such results have reduced intake efficiency levels and increased distortion at the engine face. This allowed to conclude that the dorsal intake configuration is not a viable option for aircraft that require maneuvers of high angles of attack at supersonic speeds. However, performance levels in terms of efficiency and compatibility have been shown to be promising for the aircraft's mission, as only high subsonic and transonic speeds are required, and only supersonic speeds are used in the escape trajectory phase, without needing high angles of attack.

In sum, the inlet fully integrated into the fuselage combined with the S-duct diffuser which can provide line-of-sight blockage of the engine blades has the potential to satisfy the requirement of low signature, light weight and low drag for the next generation propulsion systems.

Acknowledgments

The authors express their gratitude to Maria Luisa Bambozzi de Oliveira and Roberto Gil Annes da Silva, members of the evaluation Jury of the masters degree dissertation of Bravo-Mosquera P. D.

The authors are thankful to CAPES (Coordenação de Aperfeiçoamento de Pessoal de Nível Superior) for the scholarship granted.

References

[1] Pace S. Supersonic Cavaliers. *Airpower*, Vol. 16, No. 6, 1986.

[2] Williams T, Hunt B and Smaltzer D. Top inlet system feasibility for transonic-supersonic fighter aircraft applications. *NASA Technical Memorandum 81292*, pp 1-15, 1980.

[3] Sobester A. Trade-offs in jet inlet design: A historical perspective. *Journal of Aircraft*, Vol. 44, No. 3, pp 705-717, 2007.

[4] Rhoades W and Surber L. Top mounted inlet flow field testing for future fighter aircraft. *AIAA journal*, pp 79-1147 , 1979.

[5] Nelms W and Durston D. Concept definition and aerodynamic technology studies for single-engine v/stol fighter - attack aircraft. *In: AIAA and NASA Ames VTOL Conference*. USA, 2647, 1981.

[6] Seddon J. Boundary-layer interaction effects in intakes with particular reference to those designed for dual subsonic and supersonic performance. *Citeseer*. 1970

[7] Goldsmith E and Seddon J. Practical intake aerodynamic design. *AIAA*. 1993

[8] Seddon J and Goldsmith E. Intake aerodynamics. *AIAA*. 1999

[9] Cui D, Zhu S and Zheng R. Comparison studies for inverted and no-inverted supersonic inlets. *In: 21st AIAA International Space Planes and Hypersonics Technologies Conference*. China. p. 2300, 2017.

[10] Wan D and Guo R. Numerical simulation and experimental verification of a fixed-geometry 2D mixed-compression supersonic inlet with sweep-forward high-light and X-type missile configuration. *Journal of Aerospace Power*, Vol .22, No. 8, 2007.

[11] Zheng R, Li W, Chang J, Cui D, Man Y, Zhu S, Yu D and Chen F. Suppression of Interaction Between Shock Wave and Boundary Layer for X-Hypersonic Inverted Inlet. *Journal of propulsion technology*. Vol. 9, pp. 1153-1161. 2014.

[12] Sun Y and Smith H. Review and prospect of supersonic business jet design. *Progress in Aerospace Sciences*, Vol. 90, pp. 12-38, 2017.

[13] Flightglobal. Russia working on quiet supersonic business jet, 20 September 2012, Source: https://www.flightglobal.com/news/articles/russia-working-on-quietsupersonic-business-jet-369505/, last accessed 23.04.18.

[14] TsAGI Plans ICAO Chapter 14-compliant SSBJ, 25 July 2017, Source: https://www.ainonline.com/aviation-news/business-aviation/2017-07-25/tsagi-plans-icao-chapter-14-compliant-ssbj/, last accessed 23.04.18.

[15] TsAGI advanced projects to be demonstrated at MAKS-2017, 10 july 2017, Source: http://tsagi.com/pressroom/news/3185/, last accessed 23.04.18.

[16] Whitford R. Design for air combat. *Jane's information group*. 1987.

[17] Col. Y Udaya Chandar (Retd). The Modern Weaponry of the WorldâĂŹs Armed Forces. ISBN 978-1-946983-79-4. 2017.

[18] Roskam J. Airplane design: Parts I through VIII. *DARcorporation*. 1997.

[19] Raymer D. Aircraft design: A conceptual approach. *AIAA education series*. 1999.

[20] Lintern G, Shepard D, Parker L, Yates E and Nolan D. Simulator design and instructional features for air-to-ground attack: A transfer study. *Human Factors*, Vol. 31, No. 1, pp. 87-99. 1989.

[21] Mavris D and Delaurentis D. An integrated approach to military aircraft selection and concept evaluation. *In: Aircraft Engineering, Technology, and Operations Congress*. p. 3921. 1995.

[22] Bravo-Mosquera P D. Projeto conceitual e análise de desempenho do sistema de admissão de ar em uma aeronave não convencional de combate. *Dissertação de mestrado em Engenharia Mecânica*. Escola de Engenharia de São Carlos, Universidade de São Paulo. 2017.

[23] Mattingly J, Heiser W and Pratt D. Aircraft engine design. *American Institute of Aeronautics and Astronautics*. Inc. Reston, VA. 2002.

[24] Berra L, Slater J and Olcmen S. Conceptual redesign of the B-1B bomber inlets for improved supersonic performance. *Aerospace Science and Technology* Vol. pp. 476-483. 2015.

[25] Anderson J. Modern compressible flow: with historical perspective. Vol. 12. New York: McGraw-Hill. 1990.

[26] Barnhart P. IPAC-Inlet Performance Analysis Code. *NASA - Technical report*. NASA-CR-204130, NAS 1.26:204130, E-10800. 1997.

[27] Slater J. Design and analysis tool for external-compression supersonic inlets. *In: 50th AIAA Aerospace Sciences Meeting including the New Horizons Forum and Aerospace Exposition*. p. 16. 2012.

[28] Ran H and Mavris D. Preliminary design of a 2D supersonic inlet to maximize total pressure recovery. *In: AIAA 5th ATIO and16th Lighter-Than-Air Sys Tech. and Balloon Systems Conferences*. p. 7357. 2005.

[29] Henry J, Charles C and Stafford W. Summary of subsonic-diffuser data. *Technical Report*. NACA-RM-L56F05. 1956.

[30] Lee C and Boedicker C. Subsonic diffuser design and performance for advanced fighter aircraft. *In: Aircraft Design Systems and Operations Meeting*. p. 3073. 1985.

[31] Wendt B. The performance of a subsonic diffuser designed for high speed turbojet-propelled flight. *NASA Contractor Report*, USA, CR, v. 213410, 2004.

[32] Wong S, Riseborough E, Duff G and Chan K. Radar cross-section measurements of a full-scale aircraft duct/engine structure. *IEEE transactions on antennas and propagation*, Vol. 54,

No. 8, pp. 2436-2441. 2006.

[33] Gan W and Zhang X. Design optimization of a three-dimensional diffusing S-duct using a modified SST turbulent model. *Aerospace Science and Technology*. Vol. 63. pp. 63-72. 2017.

[34] Menter F R. Influence of freestream values on k-omega turbulence model predictions. *AIAA journal*. Vol. 30. No. 6. pp. 1657-1659. 1992.

[35] Hyoungjin K, Meng-Sing L. Shape design optimization of embedded engine inlets for N2B hybrid wing-body configuration. *Aerospace Science and Technology*. Vol. 30. No. 1. pp. 128-149. 2013.

7 Contact Author Email Address

mailto: pdbravom@usp.br

Copyright Statement